Engineered anti-inflammatory peptides inspired by mapping an evasin-chemokine interaction

Benoit Darlot[#1], James R. O. Eaton[#1,2], Lucia Geis-Asteggiante[#1], Gopala K. Yakala[#2], Kalimuthu Karuppanan[2], Graham Davies[2], Carol V. Robinson[1], Akane Kawamura*[1,2,3] and Shoumo Bhattacharya*[2]

[1]Chemistry Research Laboratory, Department of Chemistry,
[2]RDM Division of Cardiovascular Medicine,
University of Oxford, Oxford, United Kingdom

[3]Present address: School of Natural and Environmental Sciences,
Newcastle University, Newcastle upon Tyne, United Kingdom

*Corresponding authors: Akane Kawamura and Shoumo Bhattacharya
E-mail: akane.kawamura@chem.ox.ac.uk, sbhattac@well.ox.ac.uk
Joint first authors

Running title: Evasin-inspired peptides

Keywords: Chemokine, C-C motif chemokine ligand (CCL), chemotaxis, mass spectrometry, inflammation, protein-protein interaction, evasin, tick, immune response, innate immunity

Abstract

Chemokines mediate leucocyte migration and homeostasis, and are key targets in inflammatory diseases including atherosclerosis, cytokine storm and chronic auto-immune disease. Chemokine redundancy and ensuing network robustness has frustrated therapeutic development. Salivary evasins from ticks bind multiple chemokines overcoming redundancy, and are effective in several pre-clinical disease models. Their clinical development has not progressed due to concerns regarding potential immunogenicity, parenteral delivery and cost. Peptides mimicking protein activity can overcome the perceived limitations of therapeutic proteins. Here we show that peptides possessing multiple-chemokine-binding and anti-inflammatory activities can be developed from the chemokine-binding site of an evasin. We used hydrogen–deuterium exchange mass spectrometry to map the binding interface of the evasin P672 that physically interacts with C-C motif chemokine ligand 8 (CCL8) and synthesized a 16-mer peptide (BK1.1) based on this interface region in evasin P672. Fluorescent polarization and native mass spectrometry approaches showed that BK1.1 binds CCL8, CCL7 and CCL18, and disrupts CCL8 homodimerization. We show that a BK1.1 derivative, BK1.3, has substantially improved ability to disrupt P672 binding to CCL8, CCL2 and CCL3 in an AlphaScreen assay. Using isothermal titration calorimetry, we show that BK1.3 directly binds CCL8. BK1.3 also has substantially improved ability to inhibit CCL8, CCL7, CCL2 and CCL3 chemotactic function *in vitro*. We show that local as well as systemic administration of BK1.3 potently blocks inflammation *in vivo*. Identification and characterization of the chemokine-binding interface of evasins could thus inspire the development of novel anti-inflammatory peptides that therapeutically target the chemokine network in inflammatory diseases.

The disease burden created by inflammation ranges from acute multi-organ failure in influenza or coronavirus COVID19-induced cytokine storm (1-3), to chronic autoimmune diseases such as rheumatoid arthritis, and to inflammatory diseases such as atherosclerosis (4). *Chemo*-attractant cyto*kines* or *chemokines* are key players in cytokine storm hyperinflammation syndromes (1-3,5), in diverse autoimmune diseases (6), and in atherosclerosis (7). Chemokines are classified as CCL, CXCL, CX3CL or XCL based on the spacing of their *N*-terminal cysteine residues (8). The binding of chemokines to G-protein coupled receptors expressed on leucocytes causes their directed

migration to sites of inflammation, and also maintains leucocyte homeostasis (8). Although chemokines are promising therapeutic targets, clinical trials of agents that target single chemokine ligands or receptors have not been successful (9,10). The reason for this is thought, at least in part, to lie in the apparent redundancy within the chemokine network which creates robustness (11). Natural selection in diverse pathogens including viruses (12), helminths (13), and ticks (14) has resulted in the convergent evolution of structurally unrelated proteins that bind multiple chemokines. This phenomenon suggests that ability to target multiple chemokines is an effective strategy to disable the chemokine network and host defense mechanisms such as inflammation. The application of such chemokine-binding proteins in diverse pre-clinical models of inflammation has been well documented (15,16). Of particular interest in the development of therapeutics that target chemokines are the evasin proteins from ticks. Three of these proteins were initially identified in seminal studies from the Proudfoot laboratory (reviewed in (16)), and we and others have since identified and characterized over 40 evasins to date (17-21). Evasins fall into two classes, A, exclusively binding CCL chemokines, and B, exclusively binding CXCL chemokines (reviewed in (14)). When administered parenterally, evasins have potent anti-inflammatory efficacy in pre-clinical disease models including myocardial ischemia and reperfusion injury, intestinal ischemia, colitis, acute pancreatitis, lung inflammation, arthritis, psoriasis and graft-versus-host disease (reviewed in (16)). Unfortunately, the clinical translation of evasins has not progressed, in part due to the perceived limitations of using foreign proteins as biological therapeutics such as immunogenicity, requirement for parenteral delivery, and relatively high manufacturing costs (22,23). Peptidomimetic and peptide therapeutics developed from foreign proteins and mimicking their activity can overcome some of these limitations (24), and creating such agents from evasins is the driver of this work.

We have recently shown that a class A evasin EVA-P672 (here referred to as P672), identified from the tick *Rhipicephalus pulchellus*, binds several CC-class chemokines, and contains a CCL8 binding region in its *N*-terminus (20). Here we report the experimental mapping of the P672:CCL8 interface using hydrogen deuterium exchange mass spectrometry and biophysical analyses and identify a linear sequence in the *N*-terminus of P672 that binds CCL8. Using this information, we designed a series of short synthetic peptides which demonstrate promiscuous chemokine binding and neutralization activity *in vitro*. One of these peptides, BK1.3 was shown to be able to block inflammatory recruitment of neutrophils, eosinophils, monocytes and T-cells in an *in vivo* air-pouch model, induced by the pathogen-associated molecular pattern (PAMP), zymosan. Taken together, these experiments provide proof-of-concept that small biologically active peptides that target multiple chemokines and have anti-inflammatory activity can be engineered through the analysis of evasin:chemokine interactions.

Results

Hydrogen/deuterium exchange mass spectrometry reveals the P672:CCL8 complex interface

We performed peptide-resolution hydrogen/deuterium exchange mass spectrometry (HDX-MS) to characterize the interaction between P672 and CCL8. HDX-MS measures the rate of exchange of protein backbone hydrogen atoms with deuterium atoms in the solvent (25). Changes in deuterium uptake between free and complexed proteins can inform on protein-protein interfaces and conformational dynamics (26). Regions that are protected from deuterium uptake upon complex formation are shielded from the solvent typically due to involvement in inter-protein hydrogen-bonding networks that stabilize the complex (27). We measured the deuterium uptake of free P672, free CCL8 and of each protein upon complex formation. After confirming satisfactory sequence mapping and coverage of each protein (100% for P672, 96.9% for CCL8, Fig. S1), we compared the deuterium uptake of the free species with that of the P672:CCL8 complex species (5 s, 30 s, 5 min and 60 min incubation time points, Fig. S2). The results were mapped on to a homology model of the P672:CCL8 complex (Fig. 1*A*, *B*). While a large part of P672 and CCL8

showed no significant changes in H/D exchange rates, we observed significant decrease in H/D exchange in R18-S27 of CCL8 (% relative deuterium uptake (%D) ranging from -6 to -18) which lies in the *N*-terminal extended loop/β1-region (28), and in the *N*-terminal unstructured (predicted) region of P672 (E22-F32, D% up to -58%), indicating protection of these regions from solvent exposure when in complex (Fig. 1*B-D*, Fig. S2). All residues in CCL8 and most in P672 (F25-C30, F32) from these regions were protected at all time points (Fig. S2). Spectra of two representative P672 peptides showing a reduction in deuterium incorporation for this protected region upon complex formation are shown in Fig. 1*E*. An increase in relative deuterium uptake was observed for the *C*-terminal region of P672 (G87-C94, %D ranging from 15 to 18%), indicating higher exposure to solvent water after complex formation (Fig. 1*C* and Fig. S2). All HDX-MS uptake data and plots are shown in Table S1. These results indicate that the P672 (E22-F32) and CCL8 (R18-S27) regions are likely involved in P672:CCL8 complex formation. The protected regions of P672 and CCL8 overlap the binding interface predicted by the homology model of P672:CCL8 (20) suggesting that these residues are involved in protein-protein interactions. Changes in the deuterium uptake in these regions show little time-dependent change (5s - 60 min, Fig S2), in agreement with the tight-binding kinetics of P672:CCL8 interaction (K_d = 8.5 nM, residency time = 27 min) (20).

Residues E22-F32 in P672 contain a transferable CCL8 binding activity

To explore the function of P672 (E22-F32) we swapped this region with the corresponding segment of EVA1, which is a related CC-chemokine binding evasin that does not bind CCL8 (20) (Fig. 2*A*). We analysed the CCL8 binding activity of the resulting hybrid protein EVA1($P672_{22-32}$) (Fig. 2*B*) using biolayer interferometry (BLI), and found that it bound CCL8, whereas, consistent with previously reported results (20), the parental evasin EVA1 did not. Dose - titration experiments indicated that EVA1($P672_{22-32}$) bound CCL8 with modest affinity, K_d = 490 nM. Taken together with the HDX-MS analysis, these experiments confirmed that P672(E22-F32) is involved in forming protein-protein interactions with CCL8, and that this function can be transferred to another evasin.

Development of BK1.1, a CCL8 binding peptide

Guided by the HDX-MS and swapping experiments we tested a number of tiled peptide fragments spanning the E17-F32 region in P672 for CCL8 binding (Fig. 3*A*). Y21 and the four acidic residues *N*-terminal to Y21, were also included in this array, as both P672 and EVA1 share this region. To prevent disulfide bond formation, all peptides were synthesized with Cys30 replaced by Ala. These peptides were synthesized with *N*-terminal fluorescein isothiocyanate (FITC) to assess their chemokine binding affinities using a fluorescence polarization assay (BK1-6, Fig. 3*B*). The longest test peptide P672(E17-F32) was termed $BK1.1_{FITC}$, and a corresponding scrambled sequence was generated as a negative control (SCR_{FITC}). Only the full contiguous peptide ($BK1.1_{FITC,}$ displayed an increase in anisotropy upon incubation with CCL8 (at a concentration of 1 μM) compared to control, indicating a binding interaction. Interestingly, no changes in anisotropy was observed for Y21-F32 ($BK6_{FITC}$) under the conditions tested. We next used fluorescent polarization and dose-titration of CCL8 to estimate its affinity for $BK1.1_{FITC}$ (Fig. 3*C*), and found that this was relatively high (K_d =156 ± 7 nM (mean, ± s.e.m.). To further explore the mechanism of BK1.1 binding, we performed alanine-scanning mutagenesis where each residue of $BK1.1_{FITC}$ was replaced with Ala. We tested each mutant for binding to CCL8 using the fluorescent anisotropy assay to measure binding affinity. This revealed a number of key residues that contribute to CCL8 binding (Fig. 3*D*, Table S2). Significant differences were observed when aromatic residues Tyr and Phe (Tyr21, Tyr31, Phe25 and Phe32) were mutated. The Asp18 mutation also showed reduced affinity, supporting the peptide tiling data and indicating the importance of interactions outside of the Y21-F32 region. Notably, mutation of Pro27 completely abolished binding to CCL8 indicating that it has a key function.

BK1.1 disrupts CCL8 homodimerization

To further investigate the binding of BK1.1 to CCL8 we employed native mass spectrometry. Under native conditions, CCL8 exists as a homodimer (Fig. 3*E*). However, after incubation with BK1.1, both 1:1 and 2:1 species of the BK1.1:CCL8 complex were observed, together with CCL8 monomer and BK1.1. The presence of CCL8 monomer and BK1.1 species is likely due to partial dissociation of the complex. The stoichiometry observed was supported by dissociation of these complexes using higher-energy collisional dissociation (HCD). BK1.1 can thus form a stable 1:1 complex with CCL8 and disrupt CCL8 homodimerization in line with our P672:CCL8 native mass spectrometry analysis (20). Interestingly, the presence of low levels of 2:1 BK1.1:CCL8 complex indicate a possible second site of BK1.1 binding.

BK1.1 promiscuously binds three CC class chemokines

We next screened $BK1.1_{FITC}$ for binding against the 13 CC-chemokines known to bind to P672 (20) (Fig 3*F*). CCL7, CCL8 and CCL18 caused significant increase in anisotropy of the emitted light compared to the negative control CXCL1, a chemokine that does not bind P672 (20) suggesting a binding interaction between $BK1.1_{FITC}$ and these chemokines. Fluorescent polarization displacement assays with unlabeled BK1.1 confirmed its binding to CCL7, CCL8 and CCL18 (Fig. 3*G-I*).

Engineering of peptides with improved potency and promiscuous CC-chemokine binding

We next explored the role of the four acidic residues *N*-terminal to Y21, and the impact of Cys-Ala mutation introduced in BK1.1. We designed two shorter peptides from P672 residues Y21-F32, with either Ala (peptide Y21F32, C30A) or Cys (peptide Y21F32) at position 30 (Fig. 4*A*), and compared them to BK1.1 in their ability to disrupt the interaction between P672 and CCL8 using an AlphaScreen assay. We found that all three peptides significantly disrupted the interaction, with the effect of Y21F32, and BK1.1 far exceeding that of peptide Y21F32, C30A (Fig. 4*B*). We found that only Y21F32 and BK1.1 disrupted the P672 - CCL2 interaction, and that only Y21F32 disrupted the P672 – CCL3 interaction (Fig. 4*C* and *D*). These results implied that the four acidic residues *N*-terminal to Y21, and the Cys residue were important for chemokine binding. To improve chemokine binding affinity, we designed a series of peptides (BK1.2-BK1.5) based on BK1.1 (Fig. 4*A*), where we maintained the four acidic residues *N*-terminal to Y21, and also Cys at position 30. As cyclisation is known to improve conformational stability, a cyclic version BK1.2 was designed, with Cys30 cyclized to a *N*-terminal Tyr residue that was introduced (29,30). As a control we also created a non-cyclized version of this peptide, BK1.3. We assayed the binding of these peptides to CCL8 by examining their ability to disrupt the P672:CCL8 interaction using an AlphaScreen assay (Fig. 4*E* and *F*). We found that both BK1.2 (IC_{50} = 729 nM) and BK1.3 (IC_{50} = 238 nM) had significantly improved ability to disrupt the P672:CCL8 interaction in comparison to BK1.1 (IC_{50} = 59.1 μM). To explore the mechanism of enhanced activity we created further peptides BK1.4 (cyclized) and BK1.5 (linear) that lacked the *N*-terminal Tyr. BK1.4 is cyclized to Cys30 through the *N*-terminal Glu17 residue. We found that these modifications resulted in a significant reduction of binding activity in comparison to BK1.3 (Fig. 4*E* and *F*). These results suggested that cyclisation itself is not critical but instead that the *N*-terminal Tyr is important. Examination of the peptides by MS revealed that BK1.3 readily oxidized to form a disulfide-bonded dimer, whereas BK1.5 was monomeric (Fig. S3). To examine the binding profile of BK1 derivatives for other CC-chemokines, we tested their ability to inhibit P672 interactions with CCL2 and CCL3 using AlphaScreen (Fig. 4*G-J*). While BK1.1 did not inhibit, in line with the lack of binding observed against CCL2 and CCL3 in fluorescent polarization assays (Fig. 3*F*), all other BK derivatives showed good inhibition against CCL2, and weaker inhibition against CCL3. The IC_{50} of BK1.3 against CCL2 was 5.7 μM and against CCL3 was 43 μM. Isothermal titration calorimetry (ITC) (31) confirmed direct binding of BK1.3 to CCL8 (K_d = 217 nM, stoichiometry = 0.78, Fig. 4*K* and *L*).

Engineered peptides promiscuously neutralize chemokine function

We next explored the effect of BK1.1, 1.2 and 1.3 on CCL8, CCL7, CCL3 and CCL2 induced cell

migration. These chemokines were chosen as P672 has previously been shown to neutralize them in analogous experiments (20). We used the acute monocytic leukemia cell line THP-1 (32) in these studies as they express CCR1, CCR2 and CCR5 (33,34). All three receptors are activated by CCL8, CCL7 and CCL2, while CCL3 activates CCR1 and CCR5 (35). We performed these experiments with a single concentration of peptide (10 μM, Fig. 5*A*-*D*). P672 (300 nM) was included as a positive control, and a scrambled version of BK1.1 (SCR) as a negative control. We observed that BK1.1 reduced CCL8-induced migration to background levels, and had a modest, but significant effect on CCL7-induced migration, consistent with its ability to bind these chemokines in the fluorescent polarization assay (Fig. 5*A* and *B*). There was no significant effect on CCL3 induced migration (Fig. 5*C*). However, we found that it had a modest but significant effect in inhibiting CCL2 induced cell migration (Fig. 5*D*). Like BK1.1, BK1.2 and 1.3 also reduced CCL8 induced cell migration to baseline levels, and had a stronger effect on CCL7 and CCL2-induced migration (Fig. 5*A*, *B* and *D*). However, unlike BK1.1 they also significantly reduced CCL3 induced cell migration (Fig. 5*C*). We next performed dose titration experiments to establish the relative potencies (IC_{50}) of the engineered peptides against CCL8 (Fig. 5*E* and *F*). We found that BK1.1, BK1.2 and BK1.3 had IC_{50} values for CCL8 inhibition of 458 nM, 19 nM and 6.7 nM respectively, correlating well with the increased binding affinity. In comparison, the positive control, P672 had an IC_{50} of 2.6 nM. Taken together, these results indicated that the engineered peptides promiscuously neutralize different CC class chemokines, with BK1.3 possessing the most potent activity.

Engineered peptides prevent cellular chemokine binding

To explore the effect of BK1.1 and derivatives on chemokine ligand – cell interactions we developed a fluorescent-chemokine cell binding assay. Fluorescent chemokine (conjugated to AlexaFluor-647) binding to THP-1 cells results in an increase in the cellular fluorescence intensity, which is quantitatively measured using flow cytometry. In dose-response assays, we found that increasing doses of peptide would suppress CCL8-647 and CCL2-647 induced cellular fluorescence (Fig. 5*G*-*J*). IC_{50} values for BK1.1, BK1.2 and BK1.3 against CCL8-647 were found to be 5.8 μM, 630 nM and 47 nM respectively, while P672 had an IC_{50} of 21 nM (Fig. 5*G* and *H*). In similar assays IC_{50} values for BK1.1, BK1.2 and BK1.3 against CCL2-647 were found to be 45 μM, 6.3 μM and 2.2 μM respectively, while P672 had an IC_{50} of 21 nM (Fig. 5*I* and *J*). Taken together, these results indicate that the engineered peptides not only bind chemokines promiscuously, but neutralize their chemotactic function by preventing them from binding to cells.

Engineered peptide BK1.3 has in vivo anti-inflammatory activity

The above results suggested that the chemokine-neutralizing properties of the engineered peptides may translate into anti-inflammatory activity *in vivo*. To study this, we tested the lead peptide BK1.3 in a mouse short-term inflammation model. In this model, zymosan, a yeast cell wall derived PAMP, activates cytokine and chemokine production, and leucocyte infiltration, when injected into an artificially created subcutaneous air-pouch (36,37). Characterization of this model showed that Ccl9 is expressed at a high basal level but is not induced by zymosan. Ccl2, 5, 11, 12, 20, 22, 24, and Cxcl1, 2, 4, 5, 11, 13, 16 are expressed (>3 fold) at 4 hours following zymosan, and Ccl2, 5, 12, and Cxcl2, 4, 13, 16 are expressed (>3 fold) at 24 hours (Fig. S4). We injected BK1.3 and control SCR peptides, and the positive control P672 directly into the air-pouch at 0 and 9 h following zymosan injection. We characterized the air-pouch exudate using flow cytometry at 24 hours after zymosan injection to assess the severity and nature of inflammation. Both BK1.3 and P672 showed a strong and significant reduction in the number of neutrophils, eosinophils, monocytes and T-cells recruited to the air-pouch (Fig. 6*A*-*F*). We next determined if systemic administration of BK1.3 peptide would have anti-inflammatory activity. We injected BK1.3 and control SCR peptides, and the positive control P672 intra-peritoneally at 0 and 9 h following zymosan injection, and characterized the air-pouch exudate at 24 hours after zymosan injection as before. Again, both BK1.3 and P672 showed a substantial and

significant reduction in the number of neutrophils, eosinophils, monocytes and T-cells recruited to the air-pouch (Fig. 6*G-L*). These results show that the engineered peptide BK1.3 has *in vivo* local and systemic anti-inflammatory activity.

Discussion

Efforts to develop peptide or peptidomimetic agents that bind and inhibit multiple chemokines have to date been based on the sequences of chemokine-binding regions of receptors (38-40), and the unbiased identification by phage display of peptides that bind anti-receptor antibodies (41). These approaches have resulted in the identification of peptides that, where reported, bind one or more chemokines with relatively low (micromolar - millimolar) affinity. Individual peptides designed from the CCL5 heterodimer interface have been developed that efficiently disrupt heterodimerization of CCL5 with CCL17, CXCL4 and CXCL12, but are however specific for the heterodimer pair (42), and lack ability to target chemokines promiscuously. We have developed an alternative approach, which starts with the identification of promiscuous chemokine-binding proteins that have evolved in parasitic organisms to evade the host chemokine network. We followed these initial discoveries by mapping the chemokine-binding segment of one of these proteins, and then designing small peptides based on the mapped segment that not only promiscuously bind chemokines with relatively high (nanomolar) affinity but also have anti-inflammatory activity *in vivo*.

In this study we used HDX-MS and identified a 11-residue region (E22-F32) of P672 that was protected from deuterium uptake upon complexing with CCL8. Swapping this region into EVA1, an evasin that does not bind CCL8, transferred CCL8 binding activity to the hybrid protein. These results indicate that this 11-residue region binds CCL8. While the structural modelling informed the potential protein-protein interaction interface, the HDX-MS provided experimental validation and confidence which accelerated the discovery process. The HDX-MS result also indicated that CCL8 residues R18-S27, which overlap the *N*-terminal loop (C12-R24) (28), interact with P672. A key function of the *N*-terminal loop of CC chemokines is receptor binding, and it is targeted by several pathogenic chemokine-binding proteins (43). For example, the viral chemokine binding protein VV-35kDa targets K19 and R24 of CCL2 (44) and the viral chemokine binding protein vCCI targets R18 and R24 of CCL2 (45). This common mechanism suggests the convergent evolution of these proteins to target the residues found in this region. The binding of P672 to this region would competitively prevent CCL8 binding to its receptor, explaining how CCL8 function is neutralized. The *N*-terminal loop of CCL8 and other CC chemokines is also part of the homodimerization interface (28,43), and binding to this loop explains the prevention of CCL8 dimerization by P672 reported previously (20).

To develop chemokine-binding peptides based on the 11-residue segment identified by HDX-MS we initially screened a tiled array covering this segment. We found that addition of four acidic *N*-terminal residues and Tyr21 was necessary to be able to detect binding under these conditions, suggesting these acidic residues may be needed for increased affinity, or that the shorter peptides were sterically hindered from binding by the FITC moiety. Alanine scanning mutagenesis of the 16-residue peptide BK1.1 indicated that binding to CCL8 was mediated by Tyr and Phe residues, and also by the acidic residues at the *N*-terminus. Notably, Tyr and Phe are both found in protein interaction "hot-spots" (46,47), and complementarity in surface charge mediated by acidic residues can modulate protein interactions (48,49). A notable finding was that the Pro residue is critical for binding. Pro residues are found in turns (50), and can undergo cis-trans isomerization (51), making it likely that the Pro residue is of structural importance for BK1.1. We observed that BK1.1 prevents CCL8 homodimerization, suggesting that it likely employs a similar mechanism as P672 in binding CCL8, i.e. to the N-loop region. The fluorescent polarization studies reported indicate that BK1.1 also binds the chemokines CCL7 and CCL18, but not several others. The molecular mechanism of promiscuous chemokine binding by this short peptide is unclear at present and will require structural approaches for a more complete understanding.

Given the role of Pro in protein conformation, we decided to employ cyclisation as a strategy for restricting conformational flexibility. A surprising finding was that the addition of an *N*-terminal Tyr residue led to enhanced potency. This finding may be explained by the observation that Tyr residues are found in protein interaction "hot-spots" (46), and indeed Tyr and sulfoTyr are used by chemokine receptors to target the chemokine N-loop region (52). The role of the re-introduced Cys30 is supported by BK1.5, which differs by a single residue in comparison to BK1.1, and has marked improvement in affinity. The substantial enhancement of activity of BK1.3 thus likely arises from addition of Tyr and re-introduction of Cys30. In addition, it is likely that the unpredicted formation of a Cys linked dimer in BK1.3 enhances the functional affinity or avidity of the molecule. The isothermal calorimetry experiment assessing binding of BK1.3 to CCL8 indicated an unusual stoichiometry (n = 0.78). BK1. 3 is a dimer, with two presumed CCL8 binding sites, and after the first binding event we assume that the second site might be partially sterically hindered and not effectively bind to a second molecule of CCL8. This could explain how the estimated BK1.3:CCL8 stoichiometry (n=0.78) lies between 1:1 (n = 1) and 2:1 (n = 0.5).

Peptide cyclisation did not appear to enhance affinity, as evidenced by the lack of improvement of BK1.4 in comparison to BK1.5 or BK1.2 in comparison to BK1.3. This may be, in part, due to non-optimized cyclisation points and/or forced constraint. The serendipitous discoveries reported here - addition of *N*-terminal Tyr, and the dimerization consequent to the presence of an unpaired Cys residue - may be exploited in the rational design of other chemokine *N*-loop-binding peptides.

The improvement in binding to CCL8 observed in the BK1.1 – BK1.3 peptide series, as well as their ability to inhibit P672:CC-chemokine interactions (CCL8, CCL2, CCL3), correlated with increased chemokine neutralization potency and promiscuity. In cell-based chemotaxis assays we found that the improvement in binding affinity for CCL8 translated into increased potency for inhibiting CCL8-induced cell migration, as evidenced by the reduced IC_{50}. In addition to neutralizing CCL8 and CCL7, which was predicted by the BK1.1 fluorescent polarization binding study, the peptides BK1.2 and BK1.3 were also able to neutralize CCL2 and CCL3 induced chemotaxis. The inhibition of chemokine binding to cells indicate that the mechanism of neutralization is the prevention of chemokine binding to the cells, likely by preventing chemokine-receptor interactions.

A critical step in the clinical translation of novel anti-inflammatory therapeutics is the demonstration of efficacy *in vivo*, using a model where many components of the immune-inflammatory network are activated. We used a short-term inflammation model using the well characterized PAMP, zymosan, which activates TLR2 signaling (53), and results in the production of cytokines, chemokines, and complement (36,37). Our data indicate that zymosan-induced inflammation is significantly inhibited by both local as well as systemic administration of BK1.3. It is likely that the *in vivo* mechanism of action of BK1.3 includes the inhibition of CC-class chemokines which not only are chemoattractants for leucocyte recruitment, but also heterodimerize and synergize with certain CXC-class chemokines (42).

In conclusion, we have elucidated the molecular mechanism for the interaction between the tick salivary protein P672 and a target chemokine, CCL8, and have used the information to design promiscuous CC-chemokine binding peptides that bind with high affinity, neutralize chemokine action by preventing receptor binding and have anti-inflammatory activity *in vivo*. Our work indicates that peptides with promiscuous chemokine-binding and anti-inflammatory activity can be developed by studying evasin:chemokine interactions. Such peptides could provide a route to the development of new anti-inflammatory therapeutics that have relevance to not only chronic diseases such as atherosclerosis and rheumatoid arthritis, but also to acute illnesses such as influenza or COVID19-induced cytokine storm.

Experimental procedures

Reagents

All chemokines, unless otherwise stated, were purchased from Peprotech (UK). Fluorescent chemokines were purchased from Almac (UK). THP-1 cells (ECACC 88081201) were maintained in RPMI-1640 media supplemented with 10% fetal calf serum and 4 mM L-glutamine. Cultures were maintained between 3×10^5 and 1×10^6 cells/ml in a 37°C incubator with 5% CO_2. HEK 293F cells (Thermo Fisher) were maintained between 3×10^5 and 1×10^6 cells/ml in a 37°C incubator with 8% CO_2 and 130 RPM agitation in FreeStyle™ 293 Expression Medium.

Plasmids

Evasins were cloned in the expression vector pHLSec (54). P672 (N-terminal 8xHis-StrepII tag) expression vector and EVA1 (C-terminal Strep-8xHisII tag) have been described previously (20). The expression vector EVA1($P672_{21-32}$) was constructed using PCR and infusion cloning as described (17), and has a N-terminal 8xHis-StrepII tag. Plasmid sequences were confirmed by Sanger sequencing (Source Bioscience, UK). The CCL8 expression plasmid in vector pNIC-BIO3 has been described previously (20).

Protein expression

Evasin proteins were expressed as described previously using a mammalian expression system (20). Recombinant CCL8 was expressed as described previously as a SUMO fusion protein from *Escherichia coli* RosettaGamiTM 2 (DE3) cells (Novagen) (20).

Hydrogen deuterium exchange analysis

Working solutions of CCL8 and P672 were prepared at a concentration of 35 µM in 50 mM ammonium bicarbonate buffer pH=6.5. For estimation of HDX in the heterodimer state, solutions of CCL8 and P672 were mixed in a (1:1) ratio to reach a final concentration of 17.5 µM and incubated at 4°C for 1h (20). For estimation of HDX in the unbound state, working solution were diluted to 17.5 µM with 50 mM ammonium bicarbonate pH=6.5. Aliquots of 4.3 µL of heterodimer or unbound proteins were mixed with 48.2 µL of D_2O containing 50 mM ammonium bicarbonate buffer adjusted to pH=6.5 with DCl (final content of D_2O of 91.8%) and incubated for 5 s, 30 s, 5 min and 60 min at RT. HDX was quenched by adding 22.5 µL of 10% formic acid to reach a final volume of 75 µL and pH=2.5, corresponding to a final concentration of 1 µM. Samples were then rapidly flash frozen in liquid nitrogen and stored at -80°C for up to 5 days before analysis.

An Acquity M class ultra-high-performance liquid chromatographer with a nanoAcquity HDX manager coupled to a Synapt G2-Si time-of-flight mass spectrometer (Waters) was used and controlled using the MassLynx 4.1 software. Samples were loaded at 200 µL/min into an Enzymate pepsin column (2.1 mm x 30 mm, 5µm particle size) where the proteins were quickly digested at 20°C. Peptides were then captured for 2 min into a BEH C18 trap column (300 µm x 30 mm, 1.7 µm particle size) at 0°C and then separated in a BEH C18 analytical column (2.1 mm x 50 mm, 1.7 µm particle size) at 40 µL/min and 0°C under a 12 minutes linear gradient from 4 to 85% of acetonitrile with 0.1% formic acid. The MS^E approach was used for peptide mapping of non-deuterated proteins with trap collision energies of 15 to 35 V. Deuterated samples were analysed in scan mode only. Source parameters included: cone voltage 30V, capillary voltage 2.8 KV, source temperature 80°C, desolvation temperature 150°C, gas cone flow rate 80 L/h and desolvation gas 250 L/h.

The ProteinLynx Global Server 3.0.2 software was used for peptide mapping. Spectra were searched against a custom database containing the protein sequence of interest, requiring a non-specific digestion enzyme and allowing for variable modifications (i.e. N-terminus pyroglutamic acid from glutamine and deamidation or HexNAc (N-acetylhexosamine) of asparagine present in a N-X-S/T motif). Peptide identification required at least 3 fragment ion matches, the peptide presence in 4 out of 5 replicates, a retention time relative standard deviation of ≤ 5%, a precursor ion mass tolerance of 10 ppm and peptide maximum length of 30 residues. Relative deuterium uptakes % at the peptide-level were estimated using Dynamix 3.0 as the difference between the uptake (Da) observed for the complex species and the free

species divided by the maximum possible uptake of the peptide. Manual check of peptide retention time, charge state and possible peak overlap were also performed. Statistical analysis included a t-Student test and HDX rate differences ≥ 5% with a p-value ≤ 0.05 were considered significant. Residues with statistically significant increased or decreased HDX rates (see Table S1, % Relative Uptake) were mapped on to a homology model (see below) of the P672:CCL8 complex. Note that in the case of overlapping peptides, Dynamix 3.0 displays the %Relative Uptake for any given residue as the %Relative Uptake of the shortest peptide. Additionally, in the particular case of overlapping peptides of equal length, the %Relative Uptake refers to that of the peptide in which the residue is closest to the peptide C-terminus.

Homology modelling

The previously reported P672:CCL8 homology model (20), which was generated using the EVA1:CCL3 complex 3FPU (56) as template, was modified by replacing the CCL8 (homology modelled) structure with the CCL8 x-ray crystal structure 1ESR (28), using the align function in PyMol2.3.4.

Biolayer Interferometry

This was carried out as described previously using an OctetRed® system (17). Briefly, affinity determination was evaluated with chemokine concentrations typically ranging from 300 to 0.4 nM, using a non-interacting reference protein to allow for nonspecific binding to the sensor. We used ForteBio Data Analysis 9 software to process the data and calculate association (k_{on}), dissociation (k_{off}), and affinity (K_d) constants. Data with poor curve fits (R^2 < 0.9) were excluded. All biolayer interferometry experiments were performed at least three times.

Fluorescent peptides

All fluorescent peptides and scrambled (SCR) peptide were purchased from GL Biochem (Shanghai) and were synthesized using standard Fmoc solid phase synthesis to give peptides with a *C*-terminal amide. The scrambled peptide sequence EFTEVYEFDFKYDAPD is based on BK1.1. They were all deemed to be >90% pure by HPLC analysis and verified by LC-MS. Peptides were dissolved in DMSO and the concentration determined using NMR with TSP as an internal standard (57). All peptides were analysed using a Bruker Microflex LRF MALDI-TOF mass spectrometer.

Peptide synthesis in-house

Amino acids were purchased from CEM. Peptides were purified by HPLC using a Waters SFO system with a Kinetex® 5 mm EVO C18 100 Å (150 x 21.2 mm) column. All peptides were synthesized with a *C*-terminal amide on a 0.05 mmol scale using standard Fmoc protection chemistry on a CEM Liberty Blue automated peptide synthesizer. Detailed methods are provided in supporting information.

Fluorescence polarization assays

Fluorescence polarization (FP) assays were performed using a Clariostar (BMG Tech) plate reader with the supplied FITC excitation and emission filters using 96 half area well plates (Corning). The buffer used (FP assay buffer) was 50 mM HEPES, 150 mM NaCl, 0.1% BSA, 0.002% TWEEN-20, 0.2% DMSO, pH 7.4 and the final volume in each well was 30 µL. Polarization was converted to anisotropy using the equation A = (2*P)/(3-P) where P is polarization and A is anisotropy. For each peptide tested the gain was set to 35mP and adjusted to a well containing fluorescent peptide only. The polarization of the emitted light in the FITC emission channel was then determined. Experiments were performed as two technical and three biological replicates. Screening of P672 peptide fragments was achieved through incubation of each peptide (50 nM) with 1 µM CCL8 (Peprotech) for 30 minutes in FP assay buffer and the resulting anisotropy of the emitted light determined as above. The chemokine cross binding screen was performed by incubating 1 µM chemokine (Peprotech) with 50 nM $BK1.1_{FITC}$ for half an hour in FP assay buffer and the resulting anisotropy of the emitted light determined as above. To monitor $BK1.1_{FITC}$ Ala mutants of binding to CCL8, 50 nM labelled peptide was incubated with varying concentrations of recombinant CCL8 (0-25 µM, final) in 30 µL FP assay buffer for 30 minutes and the resulting anisotropy of the emitted light determined as above. The anisotropy was plotted

as a function of CCL8 concentration and fitted to the equation: $Y=Bmax*X/(K_d+X) + NS*X + Background$, where Y is the measured anisotropy, X is the concentration of CCL8 added, Bmax is the maximum binding, K_d is the equilibrium dissociation constant, NS is the slope of the nonlinear regression and Background is the anisotropy when no CCL8 is present, in GraphPad Prism. Displacement assays were carried out with CCL7, CCL8, and CCL18 (Peprotech, 1 μM). The chemokines were incubated with BK1.1 (50 μM) or SCR (50 μM) and $BK1.1_{FITC}$ (50 nM) for 30 minutes in FA buffer and the resulting anisotropy of the emitted light determined as above. For all FP assays, the experiments were carried out as two technical and three biological replicates.

Native mass spectrometry analyses

Samples were analysed using a modified Q-Exactive mass spectrometer (Thermo Fisher Scientific) for high-mass range measurements (58). CCL8 was buffer exchanged into 200 mM ammonium acetate solution (pH = 6.5). BK1.1 obtained in dimethyl sulfoxide (DMSO) was then added to the CCL8 homodimer solution in a 1:1 (CCL8 monomer:BK1.1) ratio. In all cases no more than 0.5% DMSO was present in the final mixture, and a control sample of CCL8 homodimer containing 0.5% DMSO was also analysed. Instrumental parameters were set to: capillary voltage of 1.2 KV, source temperature of 50°C and 60 V of source induced dissociation (SID). Gas phase dissociation was carried out by applying 35 and 55 V of higher-energy collisional dissociation (HCD) to the most intense charge state after isolation (25 m/z window). Spectra were acquired using a mass resolution of 60,000 for both precursor and dissociated product ions. All measurements were done in triplicate.

AlphaScreen assay

AlphaScreen® Histidine detection kit was purchased from PerkinElmer (6760619M lot: 2457886) and the assay was set up in white bottom Proxiplate™ 384 Plus microplates (PerkinElmer) following the manufacturer's instructions. The assay buffer used was 50 mM HEPES, 150 mM NaCl, 0.1% BSA, 0.01% Tween20, 1% DMSO, pH 7.5 and the final volume in each well was 20 μL. Briefly, biotinylated chemokine (recombinant, final concentration 1.25 nM (CCL8, produced in-house), 5 nM (CCL2, Almac) and 2.5 nM (CCL3, Almac) was pre-incubated at room temperature for 15 min with different concentrations of each peptide. His-tagged P672 (final concentration 2. 5 nM (CCL8), 5 nM (CCL2) and 1.25 nM (CCL3)) was then added to each well and the plate was incubated at room temperature for 30 min. Finally, acceptor and donor beads were added as a 1:1 suspension in buffer to each well and the plate was further incubated at RT for 1h. Data was obtained by reading the plate using a Pherastar FSX plate reader (excitation 680nm, emission 570nm) and was analysed using GraphPad Prism.

Isothermal calorimetry

Experiments were carried out on a TA Instruments Affinity ITC with low volume cells at 25°C and stirring at 250 rpm using a buffer system of HEPES 50 mM, NaCl 150 mM, pH 7.5. Twenty sequential 2 μL injections of BK1.3 (125 μM) into CCL8 (10 μM) were used to generate a binding isotherm for the interaction which was fitted to the independent (single-site) model using NanoAnalyze (v3.11.0).

Fluorescent chemokine/receptor blocking assay

CCL8-647 (2.5 nM, final) or CCL2-657 (1.2 nM, final) was incubated for 30 minutes with varying doses of peptide (0-100 μM, final concentration) in 50 μL assay buffer (RPMI-1640 + L-glutamine (4 mM) + 10% heat treated fetal bovine serum + 0.2% DMSO) at 37°C. This mixture was then added to 50,000 THP-1 cells in a 96-well v-bottomed plated to give a final volume of 100 μL, and everything incubated together for a further 30 minutes at 37°C. Following this time, the plate was centrifuged, the supernatant flicked off, and the cells resuspended in 150 μL ice cold PBSA. This was repeated twice more and the cells were finally resuspended in 150 μL ice cold PBSA. The median fluorescence intensity of 10,000 cells on the RL-1 channel was determined using an ATTUNE flow cytometer and plotted as function of peptide concentration and the data fitted to an inhibitor response curve with 4 parameters using GraphPad Prism. Experiments were performed as two technical and three biological replicates.

THP-1 cell migration assays
THP-1 monocyte cell migration assays were carried out as described (17). IC_{50} was calculated by fitting an inhibitor response curve with 4 parameters in GraphPad Prism. Experiments were performed as 3 technical and 3 biological replicates.

Subcutaneous dorsal air pouch model
C57BL/6J male mice (25-30 g, 8-10-week-old) were obtained from Charles River (UK). Air pouches were established at the dorsal side of the mice as described (59). Detailed methods are provided in supporting information. All animal procedures were approved by the UK Home Office and carried out in accordance with the UK Animals (Scientific Procedures) Act 1986, under project license PPL P973A60F5.

Statistical Analysis
All statistical analyses were performed using GraphPad Prism 8. The statistical significance was evaluated by one-way analysis of variance (ANOVA). P value (probability of a type I error) was adjusted for multiple comparisons with threshold (alpha) for a type I error <0.05. Unless otherwise indicated all data are represented as the mean ± s.e.m. of three independent experiments.

Data availability
Mass spectrometry proteomics data have been deposited to the ProteomeXchange Consortium via PRIDE (55) with the dataset identifier PXD019199. Reviewer account details are: Username reviewer15555@ebi.ac.uk, Password: 10jcfQze. All other data are contained within the manuscript or in supporting information. Plasmids and sequences are available on request from SB (sbhattac@well.ox.ac.uk).

Acknowledgements
This research was funded by British Heart Foundation Chair Award (CH/09/003/26631) to SB and Program Grants (RG/18/1/33351) to SB and AK, and the Oxford BHF Centre of Research Excellence (RE/13/1/30181). CVR is funded by MRC Grant No. MR/N020413/1**.** BD is funded by the EPSRC Centre for Doctoral Training in Synthesis for Biology and Medicine (EP/L015838/1). JROE is funded by a studentship from the Oxford BHF Centre of Research Excellence, AK is supported by a Royal Society Dorothy Hodgkin Fellowship. We thank Tom McAllister for advice on fluorescence polarization and ITC assays and Christopher Lynch for advice on endotoxin-free protein production.

Author Contributions
BD performed peptide synthesis, biotinylated chemokine synthesis, AlphaScreen assays and cell-based assays. JROE performed and analysed protein expression, biolayer interferometry, fluorescence polarization and cell-based experiments. LGA performed and analysed mass spectrometry experiments. GY performed and analysed all animal experiments. KK generated and provided recombinant proteins. GD developed the cell-based assays. CVR, AK and SB supervised and interpreted experiments and all authors contributed to writing the manuscript.

Conflict of Interest
The authors declare no competing interests.

References

1. Tisoncik, J. R., Korth, M. J., Simmons, C. P., Farrar, J., Martin, T. R., and Katze, M. G. (2012) Into the eye of the cytokine storm. *Microbiol Mol Biol Rev* **76**, 16-32
2. Mehta, P., McAuley, D. F., Brown, M., Sanchez, E., Tattersall, R. S., Manson, J. J., and Hlh Across Speciality Collaboration, U. K. (2020) COVID-19: consider cytokine storm syndromes and immunosuppression. *Lancet*
3. Huang, C., Wang, Y., Li, X., Ren, L., Zhao, J., Hu, Y., Zhang, L., Fan, G., Xu, J., Gu, X., Cheng, Z., Yu, T., Xia, J., Wei, Y., Wu, W., Xie, X., Yin, W., Li, H., Liu, M., Xiao, Y., Gao, H., Guo, L., Xie, J., Wang, G., Jiang, R., Gao, Z., Jin, Q., Wang, J., and Cao, B. (2020) Clinical features of patients infected with 2019 novel coronavirus in Wuhan, China. *Lancet* **395**, 497-506
4. Tabas, I., and Glass, C. K. (2013) Anti-inflammatory therapy in chronic disease: challenges and opportunities. *Science* **339**, 166-172
5. Brandes, M., Klauschen, F., Kuchen, S., and Germain, R. N. (2013) A systems analysis identifies a feedforward inflammatory circuit leading to lethal influenza infection. *Cell* **154**, 197-212
6. Garin, A., and Proudfoot, A. E. (2011) Chemokines as targets for therapy. *Experimental cell research* **317**, 602-612
7. Zernecke, A., and Weber, C. (2014) Chemokines in atherosclerosis: proceedings resumed. *Arteriosclerosis, thrombosis, and vascular biology* **34**, 742-750
8. Zlotnik, A., and Yoshie, O. (2012) The chemokine superfamily revisited. *Immunity* **36**, 705-716
9. Horuk, R. (2009) Chemokine receptor antagonists: overcoming developmental hurdles. *Nature Reviews Drug Discovery* **8**, 23-33
10. Szekanecz, Z., and Koch, A. E. (2016) Successes and failures of chemokine-pathway targeting in rheumatoid arthritis. *Nat Rev Rheumatol* **12**, 5-13
11. Mantovani, A. (2018) Redundancy and robustness versus division of labour and specialization in innate immunity. *Semin Immunol* **36**, 28-30
12. Heidarieh, H., Hernaez, B., and Alcami, A. (2015) Immune modulation by virus-encoded secreted chemokine binding proteins. *Virus Res* **209**, 67-75
13. Maizels, R. M., Smits, H. H., and McSorley, H. J. (2018) Modulation of Host Immunity by Helminths: The Expanding Repertoire of Parasite Effector Molecules. *Immunity* **49**, 801-818
14. Bhusal, R. P., Eaton, J. R. O., Chowdhury, S. T., Power, C. A., Proudfoot, A. E. I., Stone, M. J., and Bhattacharya, S. (2020) Evasins: Tick Salivary Proteins that Inhibit Mammalian Chemokines. *Trends Biochem Sci* **45**, 108-122
15. Sharif, S., Nakatani, Y., Wise, L., Corbett, M., Real, N. C., Stuart, G. S., Lateef, Z., Krause, K., Mercer, A. A., and Fleming, S. B. (2016) A Broad-Spectrum Chemokine-Binding Protein of Bovine Papular Stomatitis Virus Inhibits Neutrophil and Monocyte Infiltration in Inflammatory and Wound Models of Mouse Skin. *PLoS One* **11**, e0168007
16. Bonvin, P., Power, C. A., and Proudfoot, A. E. (2016) Evasins: Therapeutic Potential of a New Family of Chemokine-Binding Proteins from Ticks. *Front Immunol* **7**, 208
17. Singh, K., Davies, G., Alenazi, Y., Eaton, J. R. O., Kawamura, A., and Bhattacharya, S. (2017) Yeast surface display identifies a family of evasins from ticks with novel polyvalent CC chemokine-binding activities. *Sci Rep* **7**, 4267
18. Hayward, J., Sanchez, J., Perry, A., Huang, C., Rodriguez Valle, M., Canals, M., Payne, R. J., and Stone, M. J. (2017) Ticks from diverse genera encode chemokine-inhibitory evasin proteins. *The Journal of biological chemistry* **292**, 15670-15680
19. Alenazi, Y., Singh, K., Davies, G., Eaton, J. R. O., Elders, P., Kawamura, A., and Bhattacharya, S. (2018) Genetically engineered two-warhead evasins provide a method to achieve precision targeting of disease-relevant chemokine subsets. *Sci Rep* **8**, 6333
20. Eaton, J. R. O., Alenazi, Y., Singh, K., Davies, G., Geis-Asteggiante, L., Kessler, B., Robinson, C. V., Kawamura, A., and Bhattacharya, S. (2018) The N-terminal domain of a tick evasin is critical

for chemokine binding and neutralization and confers specific binding activity to other evasins. *The Journal of biological chemistry* **293**, 6134-6146
21. Lee, A. W., Deruaz, M., Lynch, C., Davies, G., Singh, K., Alenazi, Y., Eaton, J. R. O., Kawamura, A., Shaw, J., Proudfoot, A. E. I., Dias, J. M., and Bhattacharya, S. (2019) A knottin scaffold directs the CXC-chemokine-binding specificity of tick evasins. *The Journal of biological chemistry* **294**, 11199-11212
22. Boehncke, W. H., and Brembilla, N. C. (2018) Immunogenicity of biologic therapies: causes and consequences. *Expert review of clinical immunology* **14**, 513-523
23. Antosova, Z., Mackova, M., Kral, V., and Macek, T. (2009) Therapeutic application of peptides and proteins: parenteral forever? *Trends in biotechnology* **27**, 628-635
24. Lau, J. L., and Dunn, M. K. (2018) Therapeutic peptides: Historical perspectives, current development trends, and future directions. *Bioorg Med Chem* **26**, 2700-2707
25. Konermann, L., Pan, J., and Liu, Y.-H. (2011) Hydrogen exchange mass spectrometry for studying protein structure and dynamics. *Chemical Society Reviews* **40**, 1224-1234
26. Brown, K. A., and Wilson, D. J. (2017) Bottom-up hydrogen deuterium exchange mass spectrometry: data analysis and interpretation. *Analyst* **142**, 2874-2886
27. Marcsisin, S. R., and Engen, J. R. (2010) Hydrogen exchange mass spectrometry: what is it and what can it tell us? *Analytical and bioanalytical chemistry* **397**, 967-972
28. Blaszczyk, J., Coillie, E. V., Proost, P., Damme, J. V., Opdenakker, G., Bujacz, G. D., Wang, J. M., and Ji, X. (2000) Complete Crystal Structure of Monocyte Chemotactic Protein-2, a CC Chemokine that Interacts with Multiple Receptors. *Biochemistry* **39**, 14075-14081
29. McAllister, T. E., Yeh, T. L., Abboud, M. I., Leung, I. K. H., Hookway, E. S., King, O. N. F., Bhushan, B., Williams, S. T., Hopkinson, R. J., Munzel, M., Loik, N. D., Chowdhury, R., Oppermann, U., Claridge, T. D. W., Goto, Y., Suga, H., Schofield, C. J., and Kawamura, A. (2018) Non-competitive cyclic peptides for targeting enzyme-substrate complexes. *Chem Sci* **9**, 4569-4578
30. Kawamura, A., Munzel, M., Kojima, T., Yapp, C., Bhushan, B., Goto, Y., Tumber, A., Katoh, T., King, O. N., Passioura, T., Walport, L. J., Hatch, S. B., Madden, S., Muller, S., Brennan, P. E., Chowdhury, R., Hopkinson, R. J., Suga, H., and Schofield, C. J. (2017) Highly selective inhibition of histone demethylases by de novo macrocyclic peptides. *Nat Commun* **8**, 14773
31. Velazquez-Campoy, A., Leavitt, S. A., and Freire, E. (2015) Characterization of protein-protein interactions by isothermal titration calorimetry. *Methods Mol Biol* **1278**, 183-204
32. Tsuchiya, S., Yamabe, M., Yamaguchi, Y., Kobayashi, Y., Konno, T., and Tada, K. (1980) Establishment and characterization of a human acute monocytic leukemia cell line (THP-1). *Int J Cancer* **26**, 171-176
33. Parker, L. C., Whyte, M. K., Vogel, S. N., Dower, S. K., and Sabroe, I. (2004) Toll-like receptor (TLR)2 and TLR4 agonists regulate CCR expression in human monocytic cells. *Journal of immunology* **172**, 4977-4986
34. Achour, L., Scott, M. G., Shirvani, H., Thuret, A., Bismuth, G., Labbe-Jullie, C., and Marullo, S. (2009) CD4-CCR5 interaction in intracellular compartments contributes to receptor expression at the cell surface. *Blood* **113**, 1938-1947
35. Harding, S. D., Sharman, J. L., Faccenda, E., Southan, C., Pawson, A. J., Ireland, S., Gray, A. J. G., Bruce, L., Alexander, S. P. H., Anderton, S., Bryant, C., Davenport, A. P., Doerig, C., Fabbro, D., Levi-Schaffer, F., Spedding, M., Davies, J. A., and Nc, I. (2018) The IUPHAR/BPS Guide to PHARMACOLOGY in 2018: updates and expansion to encompass the new guide to IMMUNOPHARMACOLOGY. *Nucleic Acids Res* **46**, D1091-D1106
36. Coates, N. J., and McColl, S. R. (2001) Production of chemokines in vivo in response to microbial stimulation. *Journal of immunology* **166**, 5176-5182
37. El-Achkar, G. A., Mrad, M. F., Mouawad, C. A., Badran, B., Jaffa, A. A., Motterlini, R., Hamade, E., and Habib, A. (2019) Heme oxygenase-1-Dependent anti-inflammatory effects of atorvastatin in zymosan-injected subcutaneous air pouch in mice. *PLoS One* **14**, e0216405

38. Skelton, N. J., Quan, C., Reilly, D., and Lowman, H. (1999) Structure of a CXC chemokine-receptor fragment in complex with interleukin-8. *Structure* **7**, 157-168
39. Ezerzer, C., Dolgin, M., Skovorodnikova, J., and Harris, N. (2009) Chemokine receptor-derived peptides as multi-target drug leads for the treatment of inflammatory diseases. *Peptides* **30**, 1296-1305
40. Girrbach, M., Meliciani, I., Waterkotte, B., Berthold, S., Oster, A., Brurein, F., Strunk, T., Wadhwani, P., Berensmeier, S., Wenzel, W., and Schmitz, K. (2014) A fluorescence polarization assay for the experimental validation of an in silico model of the chemokine CXCL8 binding to receptor-derived peptides. *Phys Chem Chem Phys* **16**, 8036-8043
41. Houimel, M., and Mazzucchelli, L. (2013) Chemokine CCR3 ligands-binding peptides derived from a random phage-epitope library. *Immunology letters* **149**, 19-29
42. von Hundelshausen, P., Agten, S. M., Eckardt, V., Blanchet, X., Schmitt, M. M., Ippel, H., Neideck, C., Bidzhekov, K., Leberzammer, J., Wichapong, K., Faussner, A., Drechsler, M., Grommes, J., van Geffen, J. P., Li, H., Ortega-Gomez, A., Megens, R. T., Naumann, R., Dijkgraaf, I., Nicolaes, G. A., Doring, Y., Soehnlein, O., Lutgens, E., Heemskerk, J. W., Koenen, R. R., Mayo, K. H., Hackeng, T. M., and Weber, C. (2017) Chemokine interactome mapping enables tailored intervention in acute and chronic inflammation. *Sci Transl Med* **9**
43. Kufareva, I. (2016) Chemokines and their receptors: insights from molecular modeling and crystallography. *Curr Opin Pharmacol* **30**, 27-37
44. Seet, B. T., Singh, R., Paavola, C., Lau, E. K., Handel, T. M., and McFadden, G. (2001) Molecular determinants for CC-chemokine recognition by a poxvirus CC-chemokine inhibitor. *Proceedings of the National Academy of Sciences of the United States of America* **98**, 9008-9013
45. Beck, C. G., Studer, C., Zuber, J. F., Demange, B. J., Manning, U., and Urfer, R. (2001) The viral CC chemokine-binding protein vCCI inhibits monocyte chemoattractant protein-1 activity by masking its CCR2B-binding site. *Journal of Biological Chemistry* **276**, 43270-43276
46. Moreira, I. S., Fernandes, P. A., and Ramos, M. J. (2007) Hot spots--a review of the protein-protein interface determinant amino-acid residues. *Proteins* **68**, 803-812
47. Ma, B., and Nussinov, R. (2007) Trp/Met/Phe hot spots in protein-protein interactions: potential targets in drug design. *Curr Top Med Chem* **7**, 999-1005
48. Chothia, C., and Janin, J. (1975) Principles of protein-protein recognition. *Nature* **256**, 705-708
49. Lua, R. C., Marciano, D. C., Katsonis, P., Adikesavan, A. K., Wilkins, A. D., and Lichtarge, O. (2014) Prediction and redesign of protein-protein interactions. *Prog Biophys Mol Biol* **116**, 194-202
50. MacArthur, M. W., and Thornton, J. M. (1991) Influence of proline residues on protein conformation. *Journal of molecular biology* **218**, 397-412
51. Schmidpeter, P. A., Koch, J. R., and Schmid, F. X. (2015) Control of protein function by prolyl isomerization. *Biochim Biophys Acta* **1850**, 1973-1982
52. Ludeman, J. P., and Stone, M. J. (2014) The structural role of receptor tyrosine sulfation in chemokine recognition. *British journal of pharmacology* **171**, 1167-1179
53. Underhill, D. M., Ozinsky, A., Hajjar, A. M., Stevens, A., Wilson, C. B., Bassetti, M., and Aderem, A. (1999) The Toll-like receptor 2 is recruited to macrophage phagosomes and discriminates between pathogens. *Nature* **401**, 811-815
54. Zhao, Y., Bishop, B., Clay, J. E., Lu, W., Jones, M., Daenke, S., Siebold, C., Stuart, D. I., Jones, E. Y., and Aricescu, A. R. (2011) Automation of large scale transient protein expression in mammalian cells. *J. Struct. Biol.* **175**, 209-215
55. Vizcaino, J. A., Csordas, A., del-Toro, N., Dianes, J. A., Griss, J., Lavidas, I., Mayer, G., Perez-Riverol, Y., Reisinger, F., Ternent, T., Xu, Q. W., Wang, R., and Hermjakob, H. (2016) 2016 update of the PRIDE database and its related tools. *Nucleic Acids Res* **44**, D447-456
56. Dias, J. M., Losberger, C., Déruaz, M., Power, C. A., Proudfoot, A. E. I., and Shaw, J. P. (2009) Structural Basis of Chemokine Sequestration by a Tick Chemokine Binding Protein: The Crystal Structure of the Complex between Evasin-1 and CCL3. *PLoS ONE* **4**, e8514

57. Larive, C. K., Jayawickrama, D., and Orfi, L. (1997) Quantitative Analysis of Peptides with NMR Spectroscopy. *Applied Spectroscopy* **51**, 1531-1536
58. Gault, J., Donlan, J. A., Liko, I., Hopper, J. T., Gupta, K., Housden, N. G., Struwe, W. B., Marty, M. T., Mize, T., Bechara, C., Zhu, Y., Wu, B., Kleanthous, C., Belov, M., Damoc, E., Makarov, A., and Robinson, C. V. (2016) High-resolution mass spectrometry of small molecules bound to membrane proteins. *Nature methods* **13**, 333-336
59. Duarte, D. B., Vasko, M. R., and Fehrenbacher, J. C. (2016) Models of Inflammation: Carrageenan Air Pouch. *Curr Protoc Pharmacol* **72**, 5 6 1-9

Figures and Legends

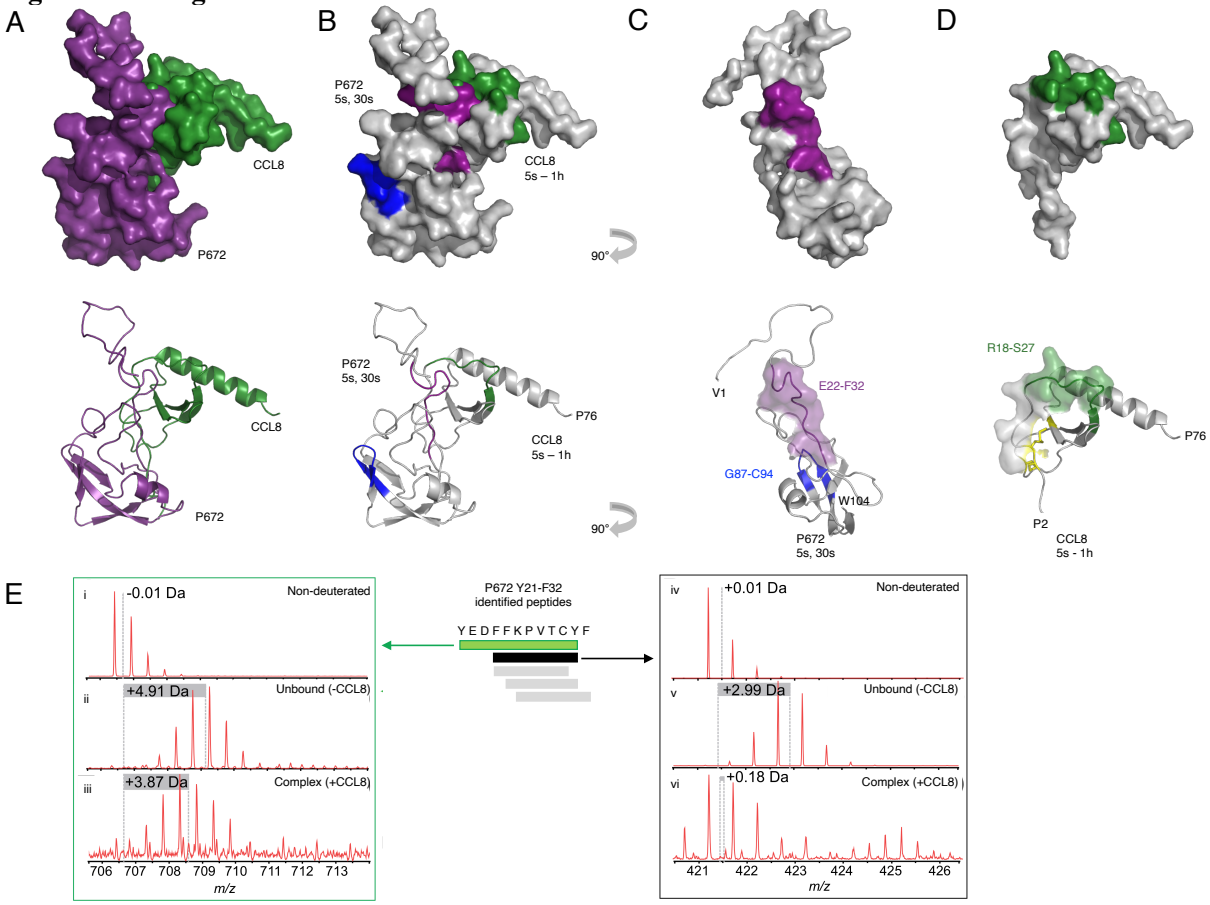

Figure 1. Characterization of CCL8/P672 interface by HDX-MS. *A,* Surface representation (top) and ribbon diagram (bottom) of a homology model of P672 (purple) and CCL8 (green) complex (see methods for details of model generation). P672 and CCL8 in 1:1 ratio was pre-incubated for 1h, then diluted in D_2O containing buffer and quenched at different time intervals (5s, 30s, 5min, 60min). *B,* Surface representation (top) and ribbon diagram (bottom) of P672 and CCL8 complex at the time points indicated. Residues with statistically significant increased HDX rates, (exposed residues, see Table S1) are shown in blue. Regions with statistically significant decreased HDX rates (protected residues, see Table S1) are shown in purple for P672 and in green for CCL8. All analyses were performed in triplicate. *C,* Surface representations (top) and ribbon diagrams (bottom) of P672 (-90° rotated view along the y-axis of *B*). Residues protected at 5s and 30s time points (E22-F32) are indicated in purple. Exposed residues (G87-C94) are indicated in blue. The surface of the protected residues (E22-F32) is also shown in the bottom panel. *D,* Surface representation (top) and ribbon diagram (bottom) of CCL8, with residues protected at all time points (R18-S27) indicated in green. Disulfide bonds are indicated in yellow. The surface of the N-loop (residues C12-R24) is also shown in the bottom panel to show the overlap with protected residues. *E,* Spectra of two representative peptides from the Y21-F32 region in P672 (green and black bars) that are protected from deuterium uptake upon complex formation. H/D exchange mass spectra were measured at t = 5s. These peptides display reduced relative deuterium uptake upon complex formation. Other peptides from this region are indicated as grey bars. Mass spectra are shown for control non-deuterated peptides (*E-i, iv*), unbound P672 deuterated peptides (*E-ii, v*), and P672 deuterated peptides when in complex with CCL8 (*E-iii, vi*).

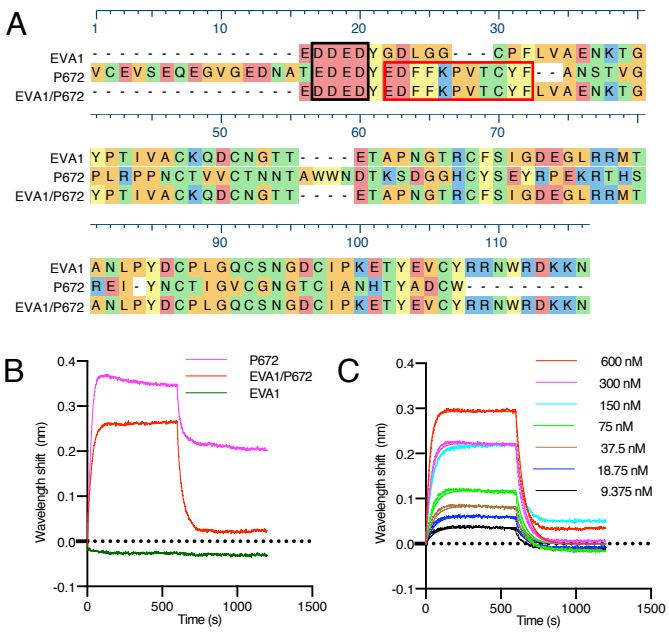

Figure 2. Design and biophysical analysis of an EVA1/P672 hybrid protein. *A,* Alignment of EVA1, P672 and EVA1/P672 (EVA1 containing $P672_{E22\text{-}E32}$) hybrid protein using MUSCLE algorithm. Amino acids are color-coded according to physicochemical properties: yellow, aromatic (F, W, and Y); red, acidic (D and E); blue, basic (R, H, and K); orange, nonpolar aliphatic (A, G, I, L, M, P, and V); green, polar neutral (C, N, Q, and T). Amino acids that were protected from deuterium uptake in P672 are indicated with a red box. The *N*-terminal acidic region is enclosed in a black box. *B,* Biolayer interferometry sensorgram obtained when either P672, EVA1/P672 or EVA1 is loaded onto the BLI sensor and exposed to 600 nM CCL8. Plots display wavelength shift (Y-axis, nm) versus time (X axis, seconds). *C,* Biolayer interferometry sensorgram for EVA1/P672 hybrid binding to CCL8. Dotted lines indicate collected data, solid lines indicate modelled data. Plots display wavelength shift (Y-axis, nm) versus time (X axis, seconds).

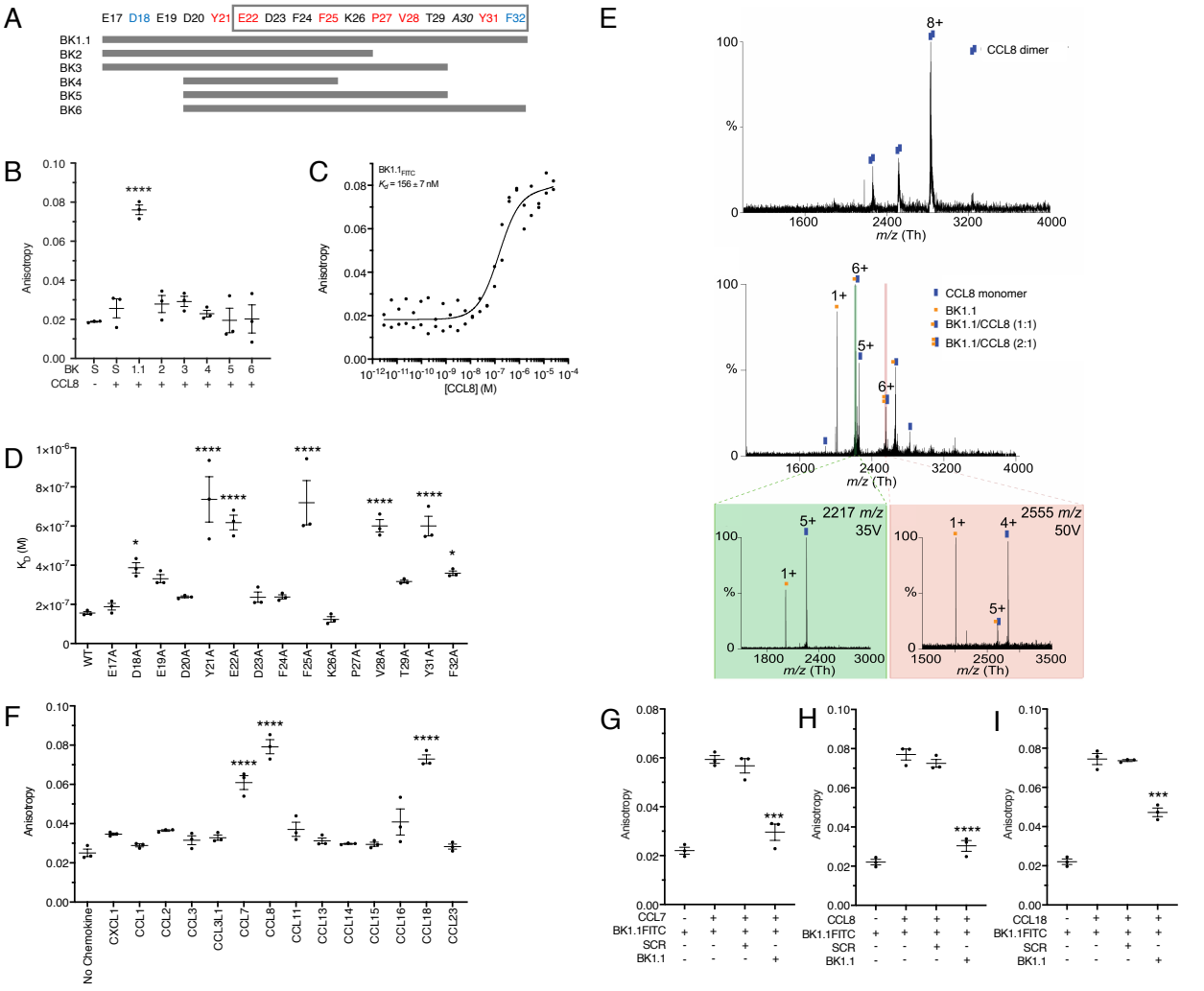

Figure 3. Development and biophysical analysis of P672-derived peptides. *A,* Design of a P672 peptide tiling array to identify CCL8-binding peptides. Positions of each residue within P672 are indicated, and the grey box indicates the CCL8 binding region identified by HDX-MS. P672 residues are colored according to CCL8 binding affinity from the Ala-scanning mutagenesis (see text and below). Red indicates either complete or highly significant loss of activity (P<0.0001), blue indicates moderately significant loss of activity (P<0.05). Peptides synthesized (BK1.1 – BK6) are indicated as grey bars. *B,* Fluorescent peptides BK1.1 – BK6 (50 nM) were incubated with CCL8 (1 μM) and the resulting anisotropy determined. A scrambled peptide (S, SCR_{FITC}) was used as a negative control. The anisotropy of each peptide after being incubated with CCL8 was compared to scrambled peptide using one-way ANOVA with Sidak's correction for multiple comparisons. **** indicates $P \leq 0.0001$. *C,* Fluorescent polarization assay to determine binding of $BK1.1_{FITC}$ to CCL8. The Y axis shows anisotropy, and X axis the dose of CCL8. Individual data points are indicated for one dataset. The curve was fitted as described in methods to calculate K_d. The mean K_d and s.e.m. of three independent experiments is shown. *D,* Fluorescent polarization assay to assess effect of alanine-scanning mutagenesis of $BK1.1_{FITC}$ on CCL8 binding. K_d values for each $BK1.1_{FITC}$ Ala mutant are shown as mean ± s.e.m of three biological replicates, which are individually indicated as points. Data for each mutant was compared to wild-type (WT) BK1.1, using a one-way ANOVA with Sidak's correction for multiple comparisons. **** = $P \leq 0.0001$, * = $P \leq 0.05$. The mutant P27A showed no detectable binding. *E,* Mass spectrometry (MS) to assess effect of BK1.1 on CCL8 *Top panel:* Native MS of CCL8 homodimer. *Mid panel:* In-solution dissociation of CCL8 dimer and further binding of CCL8 to one and two BK-1. Confirmation of CCL8/BK-1 complex by HCD gas-phase dissociation of isolated precursor ions: *Bottom*

panel, left: 2217 m/z corresponding to CCL8/BK1.1 (1:1) and *Bottom panel, left:* 2555 m/z corresponding to CCL8/BK1.1 (1:2). Buffers contained up to 0.5% DMSO. All analyses were performed in triplicate. *F,* Fluorescent polarization assay to assess the binding of $BK1.1_{FITC}$ against a CC-chemokine panel. Data are presented as mean ± s.e.m of three biological replicates, which are individually indicated as points. Each biological replicate was performed as technical duplicate. CXCL1 was used as a negative control. CC-chemokine binding compared to the negative control using a one-way ANOVA with Sidak's correction for multiple comparisons. **** = $P \leq 0.0001$, * $P<0.05$. *G-I,* Fluorescence polarization competition assay for $BK1.1_{FITC}$ and CC-chemokine interactions. $BK1.1_{FITC}$ (50 nM) was incubated with the indicated chemokine (1 μM) with or without unlabeled BK1.1 or SCR (BK1.1 scrambled) peptides (50 μM) for 30 min and the resulting anisotropy was measured. Data are presented as mean ± s.e.m of three biological replicates, which are individually indicated as points. Each biological replicate was performed as technical duplicate. Statistical significance of differences (SCR versus BK1.1) were calculated using a one-way ANOVA. **** = $P \leq 0.0001$, *** = $P \leq 0.001$.

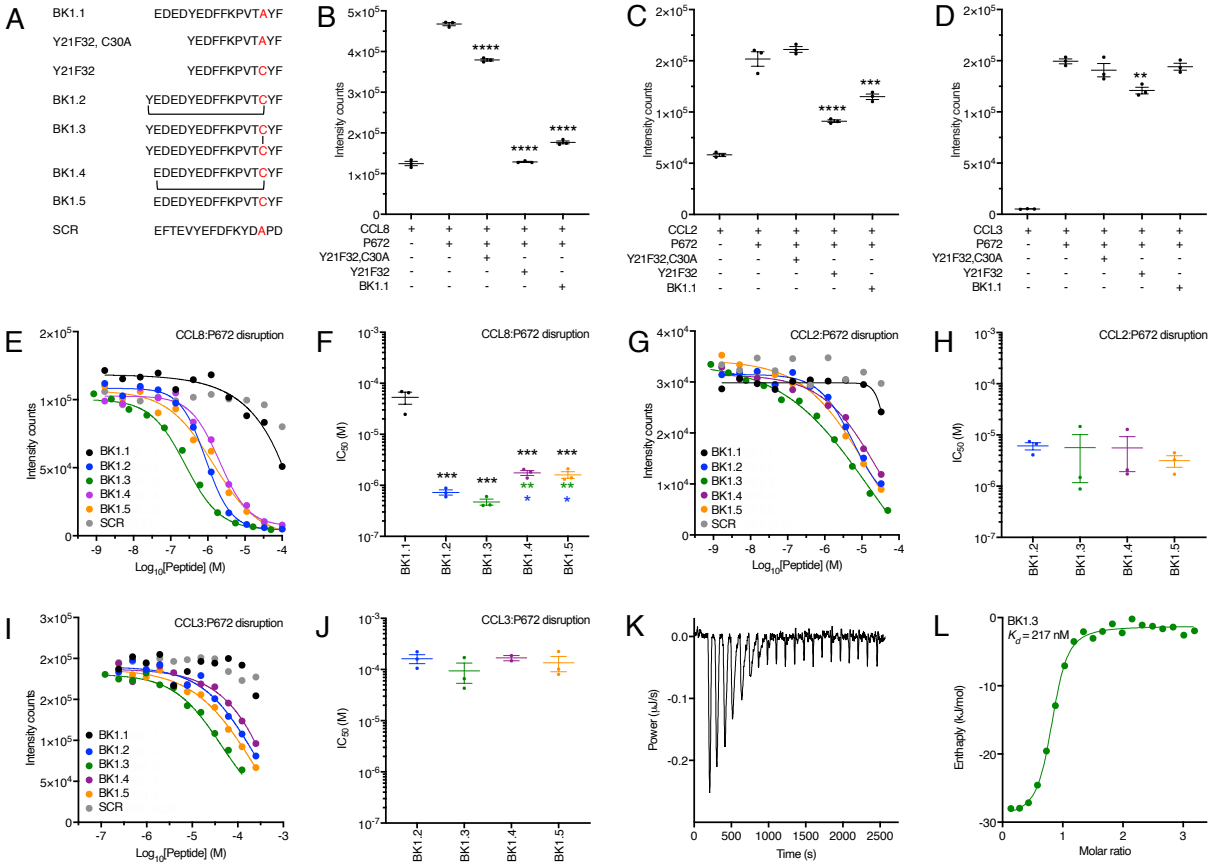

Figure 4. Development and biophysical analysis of the BK1.1 peptide series. *A,* Sequences of peptides studied, with disulfide bond (BK1.3) or thioether cyclization (BK1.2, BK1.4) indicated by lines. SCR is a scrambled peptide based on the sequence of BK1.1. *B-D,* Effect of indicated peptides at a concentration of 100 μM on a His-tagged P672 – biotinylated CCL8, CCL2 or CCL3 interaction respectively using an AlphaScreen assay. In each panel. Y axis shows intensity counts, and X axis the peptide. Data are presented as mean ± s.e.m. of three independent experiments, shown as individual data points. Statistically significant differences (compared to chemokine + P672), using a one-way ANOVA with Sidak's multiple comparisons test are indicated by asterisks. **** =P ≤ 0.0001, *** =P ≤ 0.001, **= P ≤ 0.01. *E, G, I,* Representative dose-response AlphaScreen assay curves showing disruption of His-tagged P672 interactions with biotinylated human CCL8, CCL2 and CCL3 respectively by each member of the BK1.1 derived series. Y axis shows intensity counts, and X axis the peptide concentration (Log_{10} Molar). Data are shown as mean of two technical replicates. Curves were fitted with 4 parameters to estimate IC_{50}. *F, H, J,* Summary IC_{50} values for inhibition of His-tagged P672 binding to human CCL8, CCL2 and CCL3 respectively by each member of the BK1.1 derived series, where these could be calculated. Y axis shows IC_{50} (M). Data are presented as mean ± s.e.m. of three independent experiments, each shown as individual data points. Each independent experiment was conducted as two technical replicates. Summary IC_{50} values and Hill slopes are provided in Table S3. Statistically significant differences (compared to BK1.1), using a one-way ANOVA with Sidak's multiple comparisons test, are indicated by black asterisks. Statistically significant differences (pairwise comparisons of BK1.2, BK1.3, BK1.4 and BK1.5) using one-way ANOVA with Tukey's multiple comparisons test are indicated with blue asterisks (comparisons to BK1.2), or green asterisks (comparisons to BK1.3). *** =P ≤ 0.001, **= P ≤ 0.01, *= P ≤ 0.05. *K,* Isothermal calorimetry measurements of BK1.3 binding to CCL8. Y axis shows the thermal power applied during sequential injections of BK1.3 to maintain constant temperature, and X-axis shows the time. *L.* Binding isotherm of BK1.3 binding to CCL8. Each point represents a single injection. Binding enthalpy

(kJ/mol) is shown on the Y axis, and molar ratio of BK1.3 to CCL8 on the X axis. An independent single site model (green line) was fitted to the data. Calculated thermodynamic binding parameters (± 95% confidence interval) are K_d = 217 ± 83 nM, stoichiometry n = 0.776 ± 0.024, enthalpy ΔH= -28.12 ± 1.587 kJ/mol, and entropy ΔS = 33.26 J/mol/K. Values for the blank model were 0.309 ± 0.109 μJ.

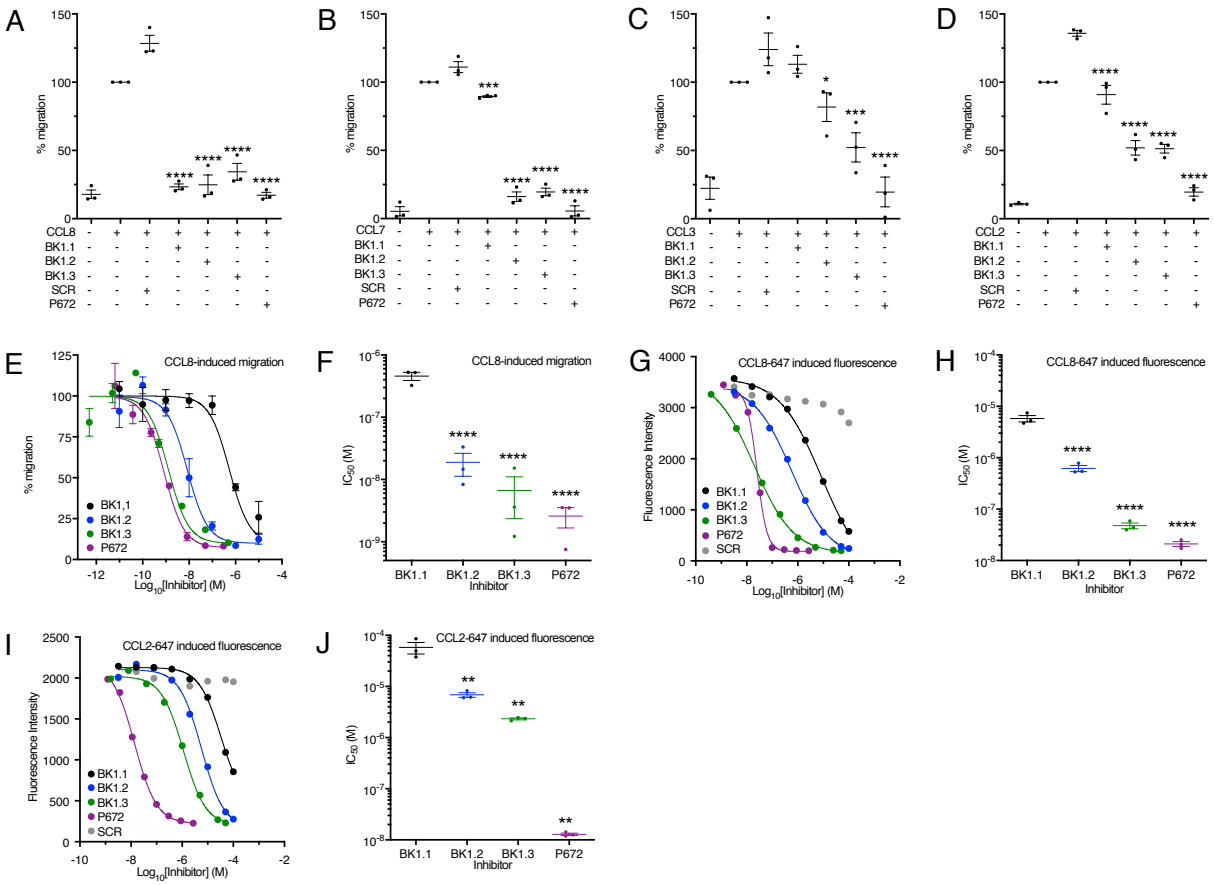

Figure 5. Cell-based assessment of P672-derived peptide activity. *A-D,* Inhibition of human chemokine induced THP-1 cell migration by BK1.1, BK1.2, BK1.3, SCR (BK1.1 scrambled, negative control) peptides, each at 10μM, and by P672 protein (positive control, 300 nM). Y axis in each panel shows % migration of THP-1 cells normalized to chemokine alone which was set at 100%. All experiments were performed at EC_{80} doses of CCL8 (5.8 nM), CCL7 (7.2 nM), CCL3 (3.5 nM), and CCL2 (1.2 nM), respectively. Data are shown as mean ± s.e.m. of three independent biological replicates, shown as individual data points. Each biological experiment was performed as three technical replicates. Statistically significant differences (compared to SCR), using a one-way ANOVA with Sidak's correction for multiple comparisons, are indicated by asterisks: **** = $P \leq 0.0001$, *** =$P \leq 0.001$, **= $P \leq 0.01$, *= $P \leq 0.05$. *E,* Representative dose-response curves showing inhibition of human CCL8 induced THP-1 cell migration by BK1.1 (black), BK1.2 (blue), BK1.3 (green), SCR (scrambled, negative control, grey) peptides and by P672 protein (positive control, magenta). Y axis shows % migration of THP-1 cells normalized to CCL8 alone which was set at 100%. Data are shown as mean ± s.e.m. of three technical replicates. X-axis shows inhibitor concentration (Log_{10} Molar). Curves were fitted with 4 parameters to estimate IC_{50}. *F,* Summary IC_{50} values for inhibition of human CCL8 induced THP-1 cell migration by BK1.1, BK1.2, BK1.3, and P672 protein. Y axis shows IC_{50} (M). Data are shown as mean ± s.e.m. of three biological replicates. Summary IC_{50} values and Hill slopes are provided in Table S3. Statistically significant differences (compared to BK1.1) using a one-way ANOVA with Sidak's correction for multiple comparisons, are indicated by asterisks: **** = $P \leq 0.0001$, *** =$P \leq 0.001$, **= $P \leq 0.01$, *= $P \leq 0.05$. *G, I,* Representative dose-response curves showing inhibition of human CCL8-647 (*G*) and human CCL2-647 (*I*) induced THP-1 cell fluorescence by BK1.1 (black), BK1.2 (blue), BK1.3 (green), SCR (scrambled, negative control, grey) peptides and by P672 protein (positive control, magenta). Y axis shows fluorescence (arbitrary units). Data are shown as mean of two technical replicates. X axis shows inhibitor concentration (Log_{10} Molar). Curves were fitted with 4 parameters to estimate IC_{50}. *H, J,*

Summary IC_{50} values for inhibition of human CCL8-647 (*H*) or CCL2-647 (*I*) induced THP-1 cell fluorescence by BK1.1, BK1.2, BK1.3, and P672 protein. Y axis shows IC_{50} (M). Data are shown as mean ± s.e.m. of three biological replicates, shown as individual data points. Each biological experiment was conducted as two technical replicates. Statistically significant differences (compared to BK1.1) using a one-way ANOVA with Sidak's correction for multiple comparisons, are indicated by asterisks: **** = $P \leq 0.0001$, *** =$P \leq 0.001$, **= $P \leq 0.01$, *= $P \leq 0.05$.

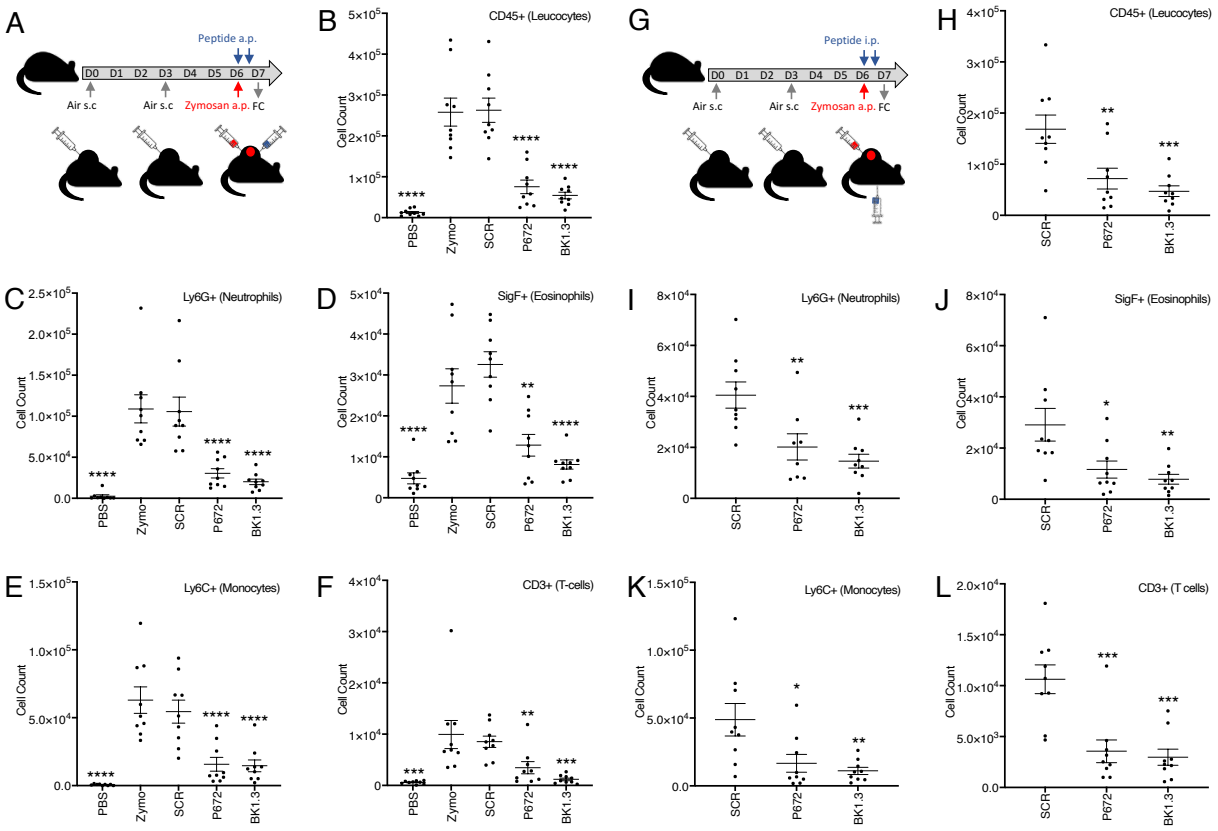

Figure 6. Assessment of anti-inflammatory activity of locally or systemically administered peptide in a mouse dorsal air-pouch model. *A,* Experimental design to assess efficacy of locally administered peptide. A dorsal air-pouch (a.p.) was created by subcutaneous (s.c.) injection of air on day 0 and day 3. Zymosan (red) or PBS (control) was injected into the air-pouch (a.p.) on day 6. Peptide or protein (blue) was injected into the air-pouch on day 6 at the time of zymosan injection and repeated 9 hours later. Air-pouch exudate was collected and analysed on day 7 by flow cytometry (FC). Nine mice were studied in each of 5 study arms: PBS alone (PBS), zymosan (zymo), zymosan + scrambled peptide (SCR), zymosan + P672 (P672), and zymosan + BK1.3 (BK1.3). *B-F,* Summary data for flow cytometry analysis for locally administered peptide. Y axis shows cell counts of total leucocytes (*B*), neutrophils (*C*), eosinophils (*D*), monocytes (*E*) and T-cells (*F*). Data are presented for each arm as mean ± s.e.m. and with individual data points. Statistically significant differences (compared to zymosan) using a one-way ANOVA with Dunnett's correction for multiple comparisons, are indicated by asterisks: **** = $P \leq 0.0001$, *** =$P \leq 0.001$, **= $P \leq 0.01$, *= $P \leq 0.05$. *G,* Experimental design to assess efficacy of intraperitoneally administered peptide. This is identical to that used for locally administered peptide (above) except that peptide or protein was administered intra-peritoneally (i.p.). Nine mice were studied in each of 3 study arms: zymosan + SCR, zymosan + P672 (P672), and zymosan + BK1.3 (BK1.3). *H-I,* Summary data for flow cytometry analysis for intraperitoneally administered peptide. Y axis shows cell counts of total leucocytes (*H*), neutrophils (*I*), eosinophils (*J*), monocytes (*K*) and T-cells (*L*). Data are presented for each arm as mean ± s.e.m. and with individual data points. Statistically significant differences (compared to SCR) using a one-way ANOVA with Dunnett's correction for multiple comparisons, are indicated by asterisks: **** = $P \leq 0.0001$, *** =$P \leq 0.001$, **= $P \leq 0.01$, *= $P \leq 0.05$.